Water Resources Research

RESEARCH ARTICLE
10.1029/2020WR027173

Wind as a Main Driver of Spatial Variability of Surface Energy Balance Over a Shallow 10^2-km^2 Scale Lake: Lake Kasumigaura, Japan

M. Sugita[1], S. Ogawa[2,3], and M. Kawade[2]

[1]Faculty of Life and Environmental Sciences, University of Tsukuba, Tsukuba, Japan, [2]Graduate School of Life and Environmental Sciences, University of Tsukuba, Tsukuba, Japan, [3]Now at Nihon Suiko Sekkei, Tokyo, Japan

Key Points:
- Spatial interpolation of meteorological variables allowed the production of seasonal, annual, and 5-year average lake energy balance maps
- Latent heat flux and total energy flux into water body exhibited pronounced spatial variability while radiative fluxes were more uniform
- The dominant northerly wind produced larger turbulent fluxes in the downwind area and hence spatial variability

Supporting Information:
- Supporting Information S1

Correspondence to:
M. Sugita,
sugita@geoenv.tsukuba.ac.jp

Citation:
Sugita, M., Ogawa, S., & Kawade, M. (2020). Wind as a main driver of spatial variability of surface energy balance over a shallow 10^2-km^2 scale lake: Lake Kasumigaura, Japan. *Water Resources Research*, *56*, e2020WR027173. https://doi.org/10.1029/2020WR027173

Received 19 JAN 2020
Accepted 6 AUG 2020
Accepted article online 10 AUG 2020

Abstract Lakes have often been treated as one-dimensional entities for energy balance (EB) studies mostly based on point measurements. Therefore, our knowledge of the spatial variability of lake EB is quite limited. We created EB maps of Lake Kasumigaura, a 172-km^2 shallow lake in Japan, with a 90-m horizontal resolution at a 3-hr interval over 5 years based on spatially interpolated meteorological variables and water surface temperature, with turbulent fluxes estimated by the bulk equations. The results indicate that turbulent fluxes and total energy flux into water body G were spatially variable while radiative fluxes were more uniform. The spatial variability of turbulent fluxes averaged over a season, a year, and 5 years was mainly caused by wind speed difference; a longer fetch in downwind areas of the lake resulted in strong winds and higher turbulent fluxes. The spatial difference of turbulent fluxes and quasi-uniform net radiation caused a total energy flux out of the water in the downwind area and a total energy flux into the lake in an upwind area. This spatial difference of G appeared to be compensated by heat transport from the upwind to downwind area through advection due to lake current.

1. Introduction

Lake surface fluxes play important roles in the formation of lake environments. For example, the lake water temperature, which is determined through energy balance (EB), is an important variable that affects many physical, chemical, and aquatic ecological processes. Also, lakes exert great influence on various features through surface fluxes in regional ecosystems; they include influence to regional climate (e.g., Lofgren, 1997; Thiery et al., 2015) and regional carbon budget (e.g., Cole et al., 2007). Therefore, there is a growing awareness in a wide range of scientific disciplines on the need to understand lake surface fluxes.

As a result, there has been an increasing number of publications which report the EB at lake's surface (e.g., Blanken et al., 2003; Franz et al., 2018; Li et al., 2015; Mammarella et al., 2015; Nordbo et al., 2011; Wang et al., 2014; Woolway et al., 2018; Zhao & Liu, 2018). However, those studies were generally based on measurements of one to several stations deployed on a lake surface. Thus, an implicit assumption in those studies is that point measurements represent a lake as a whole. Naturally, there are no obvious reasons that this should be true. As a scale of the footprint of measured fluxes is usually of the order of 10^2 to 10^3 m on water surfaces (e.g., Mammarella et al., 2015; Sugita, 2020; Zhao & Liu, 2018), spatial variability cannot be captured by single-point measurements if the lake scale is $>10^2$ to 10^3 m.

In a pioneering work of Lofgren and Zhu (2000), they demonstrated considerable spatial variabilities of monthly EB over Lake Huron (lake surface area of $A_{LAKE} = 59{,}570$ km^2), which was derived by means of the bulk equations for turbulent fluxes with the data from meteorological stations and satellite-based surface temperature. In a similar approach, Alcântara et al. (2010) presented monthly EB maps of a reservoir ($A_{LAKE} = 814$ km^2), which also illustrated the nonuniform nature of surface fluxes. Since both studies used surface temperatures determined from infrared images taken by satellites, only cloud-free cases were analyzed. It is possible that resulting monthly mean fluxes were biased toward unstable atmospheric conditions which often prevail during sunny periods. In addition, the applicability of their findings onto other lakes is somewhat limited because of the large lake size of their study areas.

According to the estimates of Downing et al. (2006), the number of lakes whose size is in the range of 10^4 to 10^5 km^2 is only three, and it is 157 in the range of 10^2 to 10^3 km^2 in the world. The target of this study is Lake

Kasumigaura, Japan, which has a surface area of $A_{LAKE} = 172$ km^2. Although this is in the same range as Alcântara et al. (2010)'s study area, $A_{LAKE} = 172$ km^2 is at the lower side. Because there is a more abundant number (=1,133) of lakes in the size range of 10^1 to 10^2 km^2, the results from this lake should have wider applicability to other lakes.

Sugita et al. (2014) and Sugita (2020) also indicated the spatial variability of surface fluxes in Lake Kasumigaura by a similar approach as Lofgren and Zhu (2000) but with a finer space resolution (90 m). In the case of Sugita et al. (2014), evaporation was studied over 5 years, but other EB components were not studied. All EB components were studied in Sugita (2020) but only for three cases on clear days in winter. It is possible that cloudy conditions suppressed spatial variability on the lake's surface. Thus, it is desirable to study spatial variability of surface EB in various sky conditions and different seasons to fully understand and generalize the spatial variability of the air-water exchange at the lake's surface.

In our study, to fill in the gap of our knowledge in the spatial variability of lake surface EB, we created fine-resolution EB maps over Lake Kasumigaura for 5 years at a 3-hr interval by extending the studies of Sugita et al. (2014) and Sugita (2020). The target fluxes include the net radiation R_n, the latent heat flux L_eE, the sensible heat flux H, and the total energy flux into lake water body G, in the EB equation at lake's surface,

$$R_n = G + L_eE + H, \tag{1}$$

in which surface is assumed to be an infinitesimally thin layer. R_n is also part of the radiation balance equation

$$R_n = R_{sd} - R_{su} + R_{ld} - R_{lu}, \tag{2}$$

where R_{sd} and R_{su} are incoming and reflected short-wave radiation, respectively, and R_{ld} and R_{lu} are incoming long-wave radiation and outgoing long-wave radiation, respectively.

2. Study Area, Data, and Methods

2.1. Lake Kasumigaura

Lake Kasumigaura (Figures 1 and S1) is the second largest lake in Japan, situated in the eastern edge of the Kanto Plain near the Pacific Ocean. Because of its location, Lake Kasumigaura is surrounded by a flat topography. The target of the study is the portion of Lake Kasumigaura commonly called Lake Nishiura (172 km^2). We will refer to it Lake Kasumigaura for this study. The average depth of the lake is 4 m. A maximum depth of approximately 7 m occurs at the center of the lake. Other relevant climatological and hydrological statistics are summarized in Table S1.

2.2. Data

2.2.1. Meteorological Data

Hourly or half-hourly data used in the analysis were wind speed, U, wind direction, relative humidity, air temperature, T, R_{sd}, and R_{ld}, measured routinely at stations in and around Lake Kasumigaura. The location and data source of the selected stations are listed in Table S2 and shown in Figure S1. The specific humidity q was determined at each station based on temperature and relative humidity.

Also used in this study was the hourly precipitation data measured at the Koshin Observatory of the Kasumigaura River Office (KRO), located at the center of Lake Kasumigaura (Figure 1), and the monthly precipitation averaged over Lake Kasumigaura derived by kriging the precipitation data of rain gauge stations in and around Lake Kasumigaura (Yamamoto, 2014). They were used to estimate the magnitude of energy input to the lake due to advection with precipitation (see section 3.1.2).

2.2.2. Surface and Water Temperature

We used water temperature T_w measurements at −0.5 m below the water surface at seven stations (see Figure S1 and Table S2 for a list) within the lake to produce the surface temperature T_s maps. The T_w values at each station were converted to T_s by adding the difference $(T_s - T_w)$ determined at the Koshin Observatory where both T_s and T_w measurements were available. A preliminary analysis was made to assess the validity of this approach by comparing the T_s maps obtained this way with those values estimated from satellite

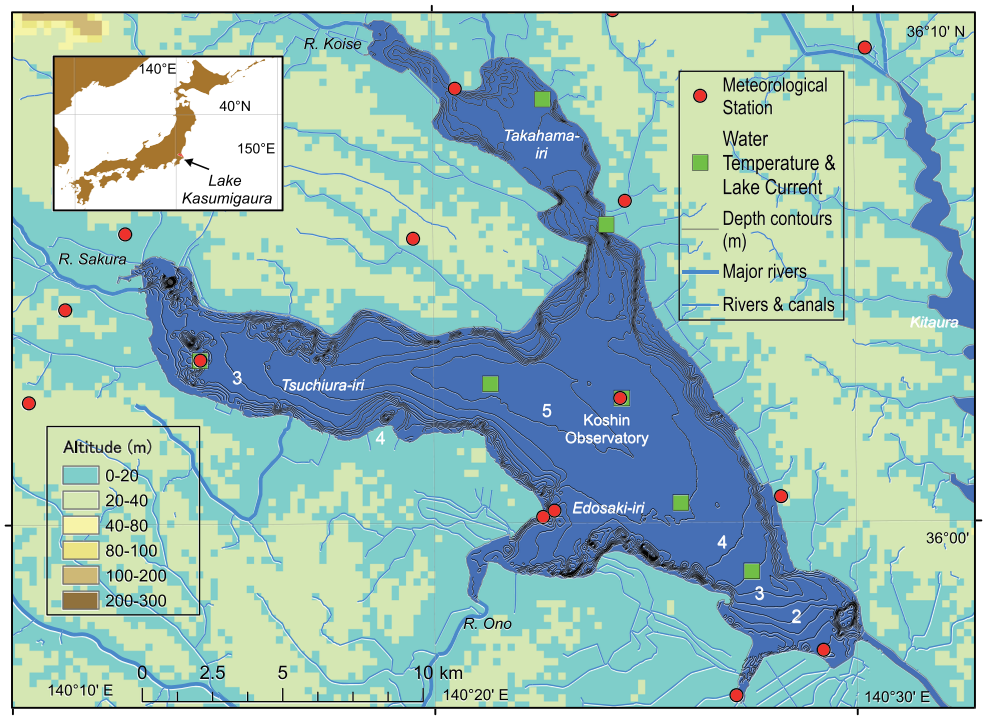

Figure 1. A map of Lake Kasumigaura. The stations whose data were used in this study are also indicated (see a map in Figure S1 for a larger area). The altitude is given in meters above sea level.

infrared images (Sugita, 2020) for the three cases. The results (Table S3) indicate that the differences between the two methods of the spatially averaged T_s values over Lake Kasumigaura are not very large (0.1–0.3°C). Similarly, H and L_eE values estimated by the method in our study (section 2.3.1) with two sets of the T_s maps are also compared in Table S3. The average flux differences are not very large (0.5–0.7 W/m^2 for H and 0–1.0 W/m^2) either. However, spatial variability as indicated by the standard deviation tends to be smaller when T_s values were estimated from T_w. This is also verified in Figure S2 which shows the differences of T_s, H, and L_eE as a map. The differences tend to be larger near the shoreline, and particularly within the northern cove (Takahama-iri, Figure 1). This appears to be because T_s was not estimated accurately near the shorelines. Thus, more number of T_w stations were needed near the shorelines to make an accurate T_s estimation. We will take this likely errors near the shorelines into consideration in the analysis of spatial variability (section 3.2).

A detail of the measurements at the Koshin Observatory is explained in Wei et al. (2016) and Sugita (2020). The surface value of specific humidity q_s was also determined by the T_s values.

2.2.3. River Discharge and Temperature

Hourly river discharge and water temperature in 2008 of three major inflow rivers (the Sakura, the Koise, and the Ono) and one outflow river (the Hitachi-tone, see Figure S1 for locations) were used to estimate energy advection due to river flows (see section 3.1.2). All the data were routinely measured and provided by the KRO.

2.2.4. Water Temperature and Lake Currents Profiles

To estimate the change of heat storage within the lake and energy advection (see section 2.3.2), we used profile data of water temperature and lake currents measured during special observations from 11 June through 10 September 2008, at seven locations within Lake Kasumigaura (INA, 2008). They were measured every 15 min at a 0.5-m interval from the lake bottom to the surface.

For the analysis of the seasonal variation of water temperature, another water profile data set was also used. They are routinely measured at eight levels from the water surface to the lake bottom by the KRO at the Koshin Observatory at a 1-month interval.

2.3. Methods

2.3.1. EB Map of Lake Kasumigaura

The entire surface of the lake was covered with 521 × 334 pixels, each with a size of 90 × 90 m. This spatial resolution was chosen to allow easy comparison with Sugita (2020) and is much finer than that of earlier studies. For example, it was 10 km in Lofgren and Zhu (2000) and 1 km in Alcântara et al. (2010). We estimated the components of Equations 1 and 2 by the methods explained below for each pixel at a 3-hr interval for 5 years of 2008–2012. The choice of the 3-hr interval was based on the result of a preliminary analysis (Table S4) in which daily mean fluxes of three 11-month data sets in 2014 were determined and compared. The three data sets consist of an hourly flux grid data set covering Lake Kasumigaura (Ogawa, 2018) and two subsets of the hourly data set sampled at 3- and 6-hr intervals. A comparison in Table S4 revealed that 3 hr were the minimum time interval that produced equally good daily mean fluxes with those of the hourly data.

An application of the bulk equations (e.g., Garratt, 1992),

$$L_eE = \rho L_e C_E U(q_s - q), \tag{3}$$

$$H = \rho c_p C_H U(T_s - T), \tag{4}$$

allowed the estimation of the turbulent fluxes of L_eE and H. C_E and C_H are the bulk transfer coefficients for water vapor and heat, respectively; U is the wind speed at 10 m; ρ is the density of air; L_e is the latent heat for vaporization; and c_p is the specific heat of air at constant pressure. Inputs to the bulk equations, U, T, T_s, and q at each pixel, were obtained through spatial interpolation of the stations' data by kriging. Ordinary kriging with a linear variogram model was used. The q_s value at each pixel was then determined from the estimated T_s value. The details of this method are explained in Sugita (2020). Sugita et al. (2014) compared hourly evaporative fluxes obtained by this method and those measured at the Koshin observatory by the eddy correlation method and reported an RMS difference of 0.03 mm/hr, which is approximately 20 W/m^2.

For C_E and C_H, Wei et al. (2016) derived empirical equations of U to estimate bulk coefficients under neutral conditions at the Koshin Observatory. They were optimized for T_s and q_s. We used these empirical equations in Equations 3 and 4 first, and then C_E and C_H were corrected through iteration for atmospheric stability by following the method of Verburg and Antenucci (2010) with a minor modification. The empirical equations of Wei et al. (2016) were estimated for open water, and thus they are not valid near the shorelines when wind direction is from the surrounding land surfaces to the lake. In such a case, the development of an internal boundary layer (IBL) should be considered. However, this was ignored in our study for the simpler treatment of grid operation. The impact of this simplification was found very small in a preliminary analysis (Table S5) when we consider the spatially averaged fluxes over Lake Kasumigaura. In this analysis, we compared the average fluxes of H and L_eE of Sugita (2020) with those obtained by the same procedure as in our study by ignoring advection effects near the shorelines. In contrast, Sugita (2020) took into consideration of the development of an IBL. Clearly, the differences of the averaged fluxes are very small ($\leq$1 W/m^2) and thus the use of Equations 3 and 4 for the whole lake's surface can be accepted when spatial mean values are considered. However, when we study spatial variation, there should be inherent errors near the shorelines where wind direction is from land to water surface although the magnitude of errors is not expected to be large as humidity above lake's surface and that above the surrounding land surfaces are not very different at Lake Kasumigaura, unlike the case over a lake in the arid climate.

We also interpolated radiative fluxes of R_{sd} and T_s measured at stations to produce pixel values. Then R_{su} at each pixel was estimated by multiplying the albedo value R_{su}/R_{sd} measured at the Koshin Observatory. R_{lu} was determined from T_s by

$$R_{lu} = \varepsilon\sigma {T_s}^4, \tag{5}$$

where ε is the emissivity and σ is the Stefan-Boltzmann constant. $\varepsilon = 1.0$ was assumed because of the uncertainty of the ε value over a lake surface where the wind speeds, turbidity, and incident angles play a role. Note that changing ε value from 1.0 to 0.97 results in -1.8 W/m^2 difference in $R_{lu} - R_{ld}$ and thus in R_n for a typical $R_{lu} - R_{ld}$ value of 60 W/m^2 and in the temperature range of 0–35°C. R_{ld} was assumed to be uniform throughout Lake Kasumigaura and we used R_{ld} measured at the Koshin Observatory for this

purpose. This assumption is likely acceptable because Hiyama et al. (1995) demonstrated the uniform spatial distribution of R_{ld} even under partly cloudy conditions over the horizontal extent of 10^2 km in this region.

Finally, R_n and G were determined by applying Equation 2 and by the rearranged form of Equation 1,

$$G = R_n - L_eE - H, \tag{6}$$

respectively. Note that errors in each term propagate into R_n and G in our method. This is likely not a problem for R_n since radiative fluxes are known to be less susceptible to measurement errors. On the contrary, turbulence fluxes of L_eE and H often exhibit large errors. Thus, such errors could go into G. This point will be discussed through EB closure in section 3.1.3.

The data sets derived above and used in this study are archived by Sugita et al. (2020).

2.3.2. Advection Terms

EB of a whole lake is expressed by

$$R_n + A_x + A_z + G_B = H + L_eE + dS/dt, \tag{7}$$

in which A_z is the vertical energy advection, A_x is the horizontal energy advection, G_B is the lake bottom heat exchange, and dS/dt is the change of energy storage within the lake water body. Heat exchange at the river-lake interface by a diffusion process is ignored in (7) since this is a minor component in comparison with A_x. In Lake Kasumigaura, A_z is solely due to precipitation $A_{z,P}$ while A_x is mainly due to discharge from rivers $A_{x,R}$ and from irrigated paddy fields $A_{x,I}$, and due to groundwater discharge $A_{x,G}$. In our study, we estimated the magnitude of $A_{z,P}$ and $A_{x,R}$ for 2008 by the following methods to compare with that of the EB components in Equation 1 while remaining advection terms in (7) were estimated through available information and findings of previous studies.

$A_{x,R}$ can be expressed by

$$A_{x,R} = \rho_w c_w \left(r_Q \sum_{i=1}^{3} T_{w,Rin,i} r_i Q_{In,i} - T_{w,Rout} Q_{Out} \right) / A_{LAKE}, \tag{8}$$

where ρ_W and c_W are the density and specific heat of water and $T_{w,Rin,i}$ and $T_{w,Rout}$ are the river water temperature of the ith inflow river and the outflow river, respectively. Similarly, $Q_{In,i}$ and Q_{Out} are the river discharge of the ith inflow river and the outflow river, respectively (section 2.2.3). The ratio r_i (in the range from1.07 to 1.46) is a conversion factor to translate discharge $Q_{In,i}$ measured at a gauging station located at some upstream distance from the lake to that at the mouth of the river by means of the area ratio of each upstream watershed. The ratio r_Q is a conversion factor from advection due to three major rivers to that by all incoming rivers and was determined from the total river discharge to the lake estimated by Yamamoto (2014) and that from the three major rivers.

The advection due to precipitation was estimated by

$$A_{Z,P} = \rho_w c_w r \sum_j T_{w,P,j} P_j, \tag{9}$$

where r is a ratio of annual precipitation averaged over Lake Kasumigaura (Yamamoto, 2014) and that at the Koshin Observatory (section 2.2.1). P_j and $T_{w,P,j}$ are the jth hourly precipitation and temperature at the Koshin Observatory, respectively. $T_{w,P,j}$ was assumed to be the same as air temperature.

2.3.3. EB Closure

To make a formal analysis to diagnose how EB is closed for a given site, the EB closure ratio (r_{EBC}) and the EB residual (R_{EB}) (Nordbo et al., 2011) are useful. They are respectively defined for a water column in Lake Kasumigaura as

$$r_{EBC} = \frac{H + L_eE}{R_n + A_{z,P} + A_{x,R} + A_{x,L} - dS/dt} \tag{10}$$

and

Table 1
Annual Mean Values of EB Components Averaged Over Lake Kasumigaura

	R_n (W/m^2)	H (W/m^2)	L_eE (W/m^2)	G (W/m^2)	$H/(R_n-G)$ (%)	$L_eE/(R_n-G)$ (%)
2008	82(±3)	21(±2)	68(±4)	−7(±7)	24	76
2009	82(±3)	20(±2)	67(±6)	−6(±5)	23	76
2010	90(±2)	21(±2)	72(±8)	−3(±8)	23	77
2011	92(±2)	20(±2)	72(±9)	0(±10)	22	78
2012	93(±2)	21(±1)	71(±8)	1(±9)	23	77
5-year	88(±2)	21(±2)	70(±6)	-3(±6)	23	77

Note. Fluxes are listed as spatial average (±standard deviation).

$$R_{EB} = R_n + A_{z,P} + A_{x,R} + A_{x,L} - dS/dt - H - LE, \tag{11}$$

where $A_{x,L}$ represents net energy input to the column due to local horizontal advection and diffusion. To apply Equations 10–11 in Lake Kasumigaura, a water column with a shape of a rectangular box with a square top (90 × 90 m, with an area of A_{top}) and rectangular side (with an area of A_{side}) centered at the Koshin Observatory was considered. $A_{x,L}$ was determined by

$$A_{x,L} = c_w\rho_w\frac{A_{\text{side}}}{A_{\text{top}}}\sum_{i=1}^{n}\left(v_{x,i}\Delta T_{w,x,i} + v_{y,i}\Delta T_{w,y,i}\right), \tag{12}$$

in which $v_{x,i}$ and $v_{y,i}$ are lake current of the ith layer in x and y directions. We ignored diffusion term in $A_{x,L}$ since a simple calculation revealed the order of magnitude of the net energy gain by the rectangular box by diffusion was 0.1 W/m^2 at most based on a typical horizontal water temperature gradient $dT_w/dx = 2 \times 10^{-4}$°C/m and reported values of diffusion coefficient (10^{-5}–10^{-2} m^2/s; Hashimoto et al., 1985; Muraoka & Fukushima, 1981) for Lake Kasumigaura. In (12), $\Delta T_{w,x,i}$ and $\Delta T_{w,y,i}$ are horizontal water temperature differences of the ith layer in x and y directions over the horizontal distance of 990 m (11 pixels). This was estimated by creating a 90-m grid of T_w for each layer covering Lake Kasumigaura by spatially interpolating profile measurements of T_w at seven locations. Since profile measurements of water temperature at fine time resolution were available only for 3 months from 11 June through 10 September (except for the period from 19 through 27 July) 2008 (section 2.2.4), we estimated the EB closure for this period based on respective cumulative EB components.

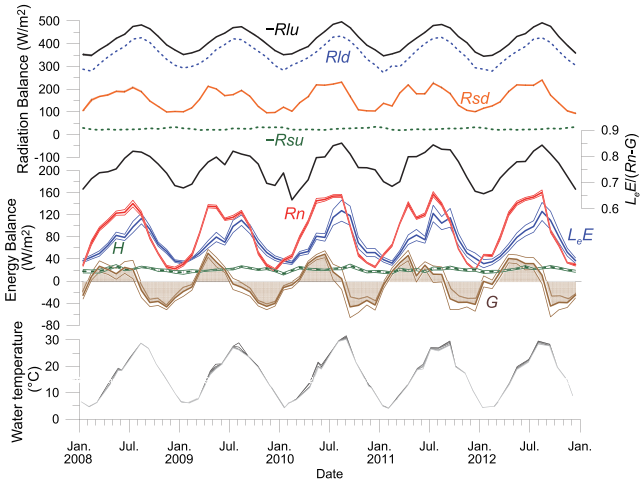

Figure 2. Monthly change of spatially averaged energy and radiation balance components and water temperature T_w at eight depths at the Koshin Observatory for 2008–2012. For the EB components, spatial averages and standard deviation over a lake surface are indicated by thick and thin lines, respectively.

3. Results and Discussion

3.1. EB of Lake Kasumigaura

3.1.1. Surface Fluxes Averaged Over the lake's Surface

Table 1 lists annual EB spatially averaged over Lake Kasumigaura. Year-to-year variations were small. A large percentage (76–83%) of R_n was distributed to L_eE while the H/R_n ratio was 22–26%. G was close to zero with an overall average of $G = -3$ W/m^2. Thus, the energy of the whole lake is essentially balanced on a yearly timescale.

Figure 2 illustrates the seasonal changes of monthly mean fluxes averaged over the lake's surface for 2008–2012 together with the water temperature at the Koshin Observatory. Year-to-year differences are not very large. The maximum and minimum R_n appeared in July–August and December, respectively. The peak of L_eE and H generally coincided with that of R_n except for 2008 when it appeared 1 month behind the R_n peak and for 2009 when there were two peaks for R_n and the second smaller peak coincided with that of L_eE. Also noticeable from Figure 2 is that the increasing rate of R_n from winter through early summer is much larger than that of L_eE and the resulting energy surplus went into lake water to increase heat storage. Thus, G was positive early spring through summer and this is the period when water temperature increased. As G turned negative, water

Table 2
Five-Year Averages of Spatially Averaged Monthly Fluxes for Different Seasons

Season	R_n (W/m^2)	H (W/m^2)	L_eE (W/m^2)	G (W/m^2)	$Bo = H/L_eE$	$EF = LE/(H + L_eE)$
JJA	138.2 ± 2.8	22.3 ± 1.1	100.7 ± 8.5	15.3 ± 8.5	0.22	0.82
JAS	126.2 ± 2.8	23.7 ± 1.4	109.7 ± 10.3	−7.2 ± 10.7	0.22	0.82
SON	59.9 ± 1.4	22.1 ± 1.7	76.8 ± 8.2	−39.0 ± 9.1	0.29	0.78
DJF	7.8 ± 0.7	6.1 ± 0.7	13.8 ± 1.7	−12.1 ± 2.1	0.44	0.70
MAM	114.2 ± 2.9	20.9 ± 1.7	64.8 ± 5.1	28.5 ± 5.6	0.32	0.76

Note. Fluxes are expressed by spatial average ± standard deviation. JJA = June–August; JAS = July–September; SON = September–November; DJF = December–February; MAM = March–May.

temperature began decreasing. This is also indicated in Table 2 in which seasonal averages of the EB components are listed. During the summer–winter period, G was negative. The stored energy was released and used to maintain L_eE and H even after R_n started decreasing. Thus, the minimum values of L_eE and H lagged behind the R_n minimum by 1–2 months. This kind of phase shift in turbulent fluxes over a lake is quite common where clear seasonal changes exist (e.g., Rimmer et al., 2009; Zhao & Liu, 2018).

As a result of different seasonal behavior of G, R_n, and turbulence fluxes, the L_eE/R_n ratio changed from around 0.5 to 2.0. The evaporative fraction $L_eE/(R_n - G)$ was more stable with a minimum value of around 0.7 in January–February and a maximum value of 0.8 in the July–August period (Figure 2) with corresponding Bowen ratio B_o of 0.4 and 0.2.

Note that the evaporative fraction can also be expressed by $\alpha\Delta/(\Delta + \gamma)$ in which Δ is the slope of the saturation vapor pressure curve at air temperature T; γ is the psychrometric constant at T; and α is the Priestley-Taylor coefficient (Garratt, 1992; Priestley & Taylor, 1972). If we assume $\alpha = 1.26$ and we take monthly mean T values in 2008–2012, $\alpha\Delta/(\Delta + \gamma) = 0.6$ in January–February and 0.9 in July–August can be obtained. They are similar to the evaporative fraction determined above. To make a perfect agreement, a larger $\alpha = 1.45$ in January–February and a smaller $\alpha = 1.12$ in July–August would be required. This is not surprising as Lake Kasumigaura is surrounded by land surfaces and the minimum advection conditions, which is the basis for $\alpha = 1.26$, should not be expected. This kind of seasonal change of α has also been reported in numerous studies (e.g., DeBruin & Keijiman, 1979).

EB characteristics found in Lake Kasumigaura can be compared with those of other lakes to highlight the difference. For this purpose, a comparison with those values reported in Woolway et al. (2017, 2018) is useful as the turbulence fluxes and other relevant variables of 39–45 lakes in various parts of the world were compared and plotted against lake surface area (A_{LAKE}) and latitude (φ). Since the target period of their studies is from July through September, the same variables were determined for this period for Lake Kasumigaura for comparison (Table 2).

We found our values to be generally within a scatter of points of other lakes plotted against A_{LAKE} and φ. However, our H and L_eE values were on a larger side while B_o was in the middle of a scatter of Figures 5 and 7 of Woolway et al. (2018). The larger fluxes were due to larger vertical differences of $\Delta T = T - T_s$, $\Delta q = q - q_s$. U and bulk transfer coefficient (C_E and C_H) were about the same. One reason for our larger ΔT and Δq is the difference in "surface" values. Theirs was water temperature T_w at 0–1 m depth (a mean of about 0.5 m) while ours was the surface skin temperature T_s. They are not always the same (e.g., Prats et al., 2018). In fact, at the Koshin Observatory, we obtained the average difference $\overline{(T_w - T_s)} = -2.5$°C between T_w at −0.5 m and T_s during the July–September period in 2008. For annual averages, this difference became smaller and was −1.9°C (with the daytime (9–15 hr) mean of −2.9°C and nighttime (1–6 and 18–24 hr) mean of −1.4°C).

Woolway et al. (2018) also showed monthly variations of H, L_eE, and B_o (the average and the standard deviation) for the 14 lakes where annual data were available. Comparison of Figures 3 and S1 of Woolway et al. (2018) with our results indicated that the magnitude and the range were quite different even though the seasonal change pattern of them was quite similar. Our H values were generally larger. We found our L_eE larger in summer and smaller in winter while our B_o was about the same with theirs in summer and

larger in winter. Thus, the annual ranges of L_eE and B_o of Lake Kasumigaura were also larger. This is expected since our study area is in a temperate climate with clearly marked four seasons while the 14 lakes are located not only in a temperate climate but also in the tropics where seasonal changes are small to absent.

3.1.2. Energy Inputs and Outputs Due to Advection

In the EB equation of a whole lake, the horizontal energy advection due to groundwater discharge $A_{x,G}$ is likely small as net groundwater inflow to the lake has been reported to be only about 1% of the total river inflow to the lake (Muraoka, 1981; Naito, 2008), due to flat topography and resulting small hydraulic gradient around Lake Kasumigaura. The influence of the horizontal energy advection due to irrigated water discharge $A_{x,I}$ is uncertain but is also expected to be not very large because the discharge from paddy fields to the lake has been estimated as 10% of the total river discharge (Yamamoto, 2014). The lake bottom heat exchange G_B is probably small since the vertical gradient of water temperature near the lake bottom is quite small (see also Figure 2) and solar energy does not reach deep into lake bottom because of low water transparency ($\leq$1 m). According to the estimate of Ogawa (2018), the downward shortwave radiation at the lake bottom is <1 W/m^2. However, there may be a seasonal variation of temperature differences between lake bottom soils and lake water, and resulting nonzero fluxes. This is because there is a difference in heat contents between water and soils and as a result, seasonal change of soil temperature may lag behind that of water temperature. Unfortunately, it is not possible to provide the magnitude of such fluxes since we do not have soil temperature data at the lake bottom.

The energy input by river advection averaged over the water surface of a year in 2008 was estimated to be 17 W/m^2 while energy output was 20 W/m^2, which result in the net energy loss of 3 W/m^2. Thus, this is an order of magnitude smaller than the annually averaged fluxes of R_n, H, and L_eE. Seasonally, it was positive from July through October while in other months it was negative (i.e., net energy loss from the lake). The above results were obtained as averages over a year and by considering Lake Kasumigaura as a well-mixed water body. It is expected that advection impact could be large locally near the river mouths and at the time of large runoff events.

We determined the average value of the vertical energy advection due to precipitation $A_{z,P}$ as 3 W/m^2 in 2008. This is a plain annual average over the periods that include both rainy and rain-free periods. So, on average, this is not a large contribution to the whole lake EB. However, this can be significant during heavy rainfall events.

Although the analysis presented above is not thorough, it is likely that the advection term in the EB equation is not very large in Lake Kasumigaura when we consider a long-term means over a year or more. In a short period, when there are heavy rainfall and large runoff events, or when rapid temperature changes occur, advection could be a major component and therefore it may not be ignored.

3.1.3. EB Closure and Estimation Errors of the EB Components

As mentioned in section 3.1.1, the fact that annual averaged G was close to zero implies that EB was closed at the lake's surface on average. This was further studied by estimating the EB closure ratio (r_{EBC}) and the EB residual (R_{EB}) for about 2 months (section 2.3.3). The resulting values were $r_{EBC} = 97\%$ and $R_{EB} = 3$ W/m^2, which are compatible with those reported in previous studies (see, e.g., Table 1 of Wang et al., 2014). Note that if we ignored the advection term due to precipitation $A_{x,P}$, that due to river discharge $A_{x,R}$, and that due to local horizontal advection $A_{x,L}$ in Equations 10 and 11, the results would be $r_{EBC} = 95\%$ and $R_{EB} = 6$ W/m^2. Thus, EB can be considered approximately closed in Lake Kasumigaura.

It is interesting to compare the R_{EB} value obtained above with the error estimates given in previous sections. An order of magnitude of the error of H and L_eE by ignoring the development of the IBL at the land-lake interface is -0.4 and -0.7 W/m^2, respectively (Table S2). The error of H and L_eE by the use of the T_s maps estimated from T_w station data is -0.5 and -0.6 W/m^2, respectively (Table S3). These can be added together to obtain -2.2 W/m^2 which is of the same order of magnitude with R_{EB}. Needless to say, however, the total error estimation given here is crude as the error components were estimated for different periods. To fully understand the error sources and the propagation of the errors into the final results, it is necessary to estimate all error sources and their magnitude for the same period of the EB study.

Table 3
Range of the Spatial Standard Deviation and Coefficient of Variation of Monthly Mean Fluxes Over Lake Kasumigaura for the 2008–2012 Period

	R_n	H	L_eE	G
Range of the standard deviation, s (W/m^2)	1–6	1–4	1–19	4–20
Range of the absolute value of the coefficient of variation, |CV|	0.01–0.15	0.05–0.23	0.04–0.24	0.11–15.88

Note. CV is defined as the standard deviation divided by the average.

3.2. Spatial Variation of Surface EB Components

3.2.1. Monthly, Seasonal, Annual, and 5-Year Averages

Tables 1 and 2 list the spatial standard deviation s of the annual and seasonal mean EB components over Lake Kasumigaura, while Figure 2 indicates the monthly change of s. The range of the monthly change of s and the absolute value of the coefficient of variation |CV| is listed in Table 3. They indicate that the spatial variability of the absolute value of flux was smaller for R_n and H in comparison with L_eE and G. For R_n, |CV| was also small. In contrast, |CV| for H was comparable with that for L_eE. This implies that the mechanism behind the spatially nonuniform distribution of H and L_eE was likely the same. The small spatial variability of R_n reflects that of R_{sd}.

These results indicate that it is important to take horizontal variability of surface EB into consideration for accurate estimation of the average (or the total) flux of a lake. In fact, if we assumed that measurements at the Koshin Observatory represent the whole lake, the resulting fluxes would be different from those obtained as spatially averaged fluxes. For 5-year averages, this difference was 3 W/m^2 (3% error) for R_n, 2 W/m^2 (10% error) for H, 6 W/m^2 (9% error) for L_eE, and 5 W/m^2 (167% error) for G. The error becomes larger as we choose shorter averaging period. For the daily averages, the mean absolute difference is 5 W/m^2 (6% error) for R_n, 4 W/m^2 (18% error) for H, 11 W/m^2 (15% error) for L_eE, and 15 W/m^2 (520% error) for G.

Figure 3 illustrates the spatial distribution of scaled values of EB components averaged over the 5 years. Fluxes were made nondimensional by $y = (x - \overline{x})/s_x$ to allow easy comparison of fluxes with different magnitude. In the equation, x represents one of R_n, H, L_eE, or G and s_x is the standard deviation of x. An alternative version of Figure 3 is given in Figure S3 which shows flux maps in the unit of W/m^2.

It is quite clear that EB components, particularly H and L_eE, were spatially nonuniform. This is so even if we take likely estimation errors near the shorelines (sections 2.2.2 and 2.3.1) into consideration. The turbulent fluxes exhibit larger values in the southern part although the area with larger H extends further to the north. There was also a spatial variability in R_n. However, its actual magnitude was small (Table 1, Figures 2 and S3) as mentioned above. So in a relative sense, R_n was quasi-uniform while H and L_eE were not. As a result, the spatial difference of G was determined mostly by the spatial distribution of H and L_eE (and in particular L_eE since $H < L_eE$). G was positive to the northern and western parts of the lake while a negative part appeared from the center of the lake to the south-southeastern end. Comparisons of Figure 3 with maps of relevant variables in Equations 3–4 (not shown, except for the wind speed U in Figure 4a) indicated that a main cause of this spatial variation was the difference in U. An area of larger values of U exists from the center to the southern end of Lake Kasumigaura. This spatial difference was caused by dominant wind directions (N to NE) in this area. Winds gained speed along the fetch over the lake's surface in general N-S direction and as a result, larger turbulent fluxes can be found in southern parts.

Because of the spatial variability of G, lake water received energy and was heated in the northern and western parts while energy was lost and water was cooled in the southern parts, on average over a long period. This was probably accompanied by energy advection by lake currents from north to south through the center of the lake and its compensating flow from south to north along the shorelines as observed by INA (2008) under the northerly wind condition (Sugita, 2020). In other words, the energy surplus in the north was transported to the south where it was lost by negative G values. This is schematically shown in Figure 5 which illustrates north-south cross-section of the lake with vertical fluxes, wind direction, and wind speed.

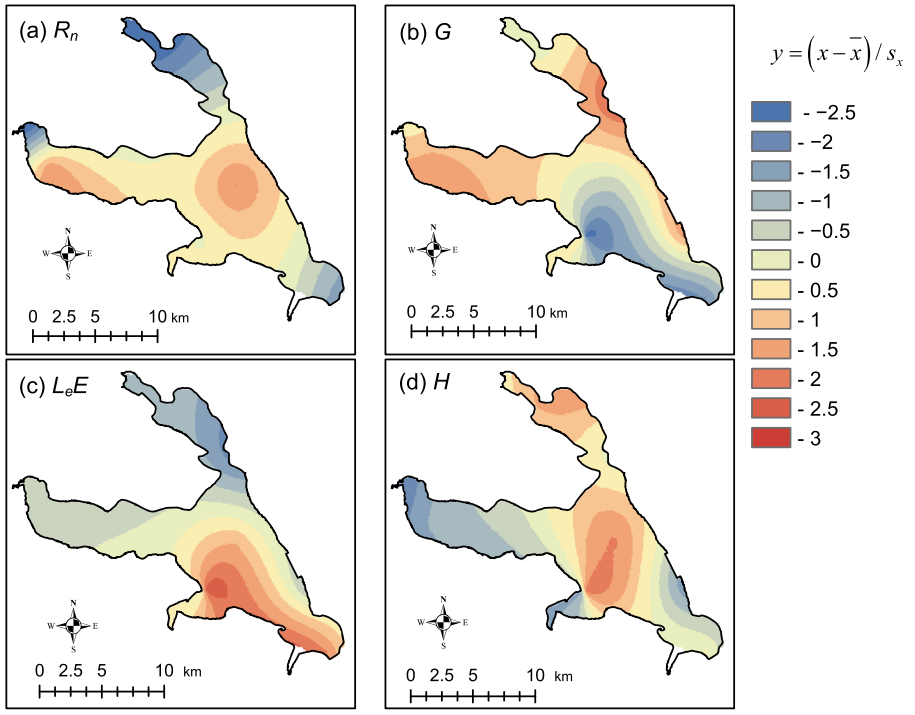

Figure 3. Spatial variation of 5-year averaged (a) net radiation, (b) total flux into water body, (c) latent heat flux, and (d) sensible heat flux. Fluxes x are shown as a nondimensional variable $y = (x - \bar{x})/s_x$ where $\bar{x}$ and s_x are the spatial average and the standard deviation.

R_n was about the same both in the northern and southern parts while L_eE was larger in the southern part due to stronger wind which gained speed along the fetch over the lake's surface. Since the magnitude of H was smaller than that of the other EB components, G was mainly determined by the balance between R_n and L_eE. This resulted in positive G in the northern part and negative G in the southern part.

Figure 6 shows the spatial variation of G averaged over each of four seasons. Corresponding figures for U are shown in Figures 4b–4d. The general pattern of gradual decrease of G from north to south is consistent through four seasons (except perhaps for the December–February period when the area of minimum G appeared at the center of the lake), but the magnitude of G changed. In spring (March–May), $G > 0$ over the whole lake's surface. In summer (June–August), the area with $G < 0$ began to appear in the southern part, and this area expanded to the whole lake surface in fall (September–November) and winter (December–February).

3.2.2. Sky Condition and Spatial Variability

The results presented in section 3.2.1 have indicated that wind is a major factor to determine the spatial variability of the EB components. This is somewhat different from the conclusions obtained in Sugita (2020) which showed not only the wind speed but also the vertical differences of temperature and humidity are important to control the spatial distribution of H and L_eE. As explained in section 1, Sugita (2020) studied EB on clear days as T_s from satellite images were used. On the contrary, the analysis in section 3.2.1 is for long-term averages that include both clear and cloudy conditions. It is natural to suspect that sky condition influences the spatial variability and its controlling factors.

To investigate this possibility, three cloudy cases were selected and compared with the corresponding three clear sky cases in Sugita (2020). The three cases were different in wind speeds. The cloudy condition was judged by the zero sunshine duration at the Koshin Observatory. The results are summarized in Table 4 together with those from Sugita (2020).

The comparison immediately reveals that the CV values of H and L_eE under cloudy conditions are smaller than those under clear conditions, indicating that spatial variability is weaker under cloudy conditions,

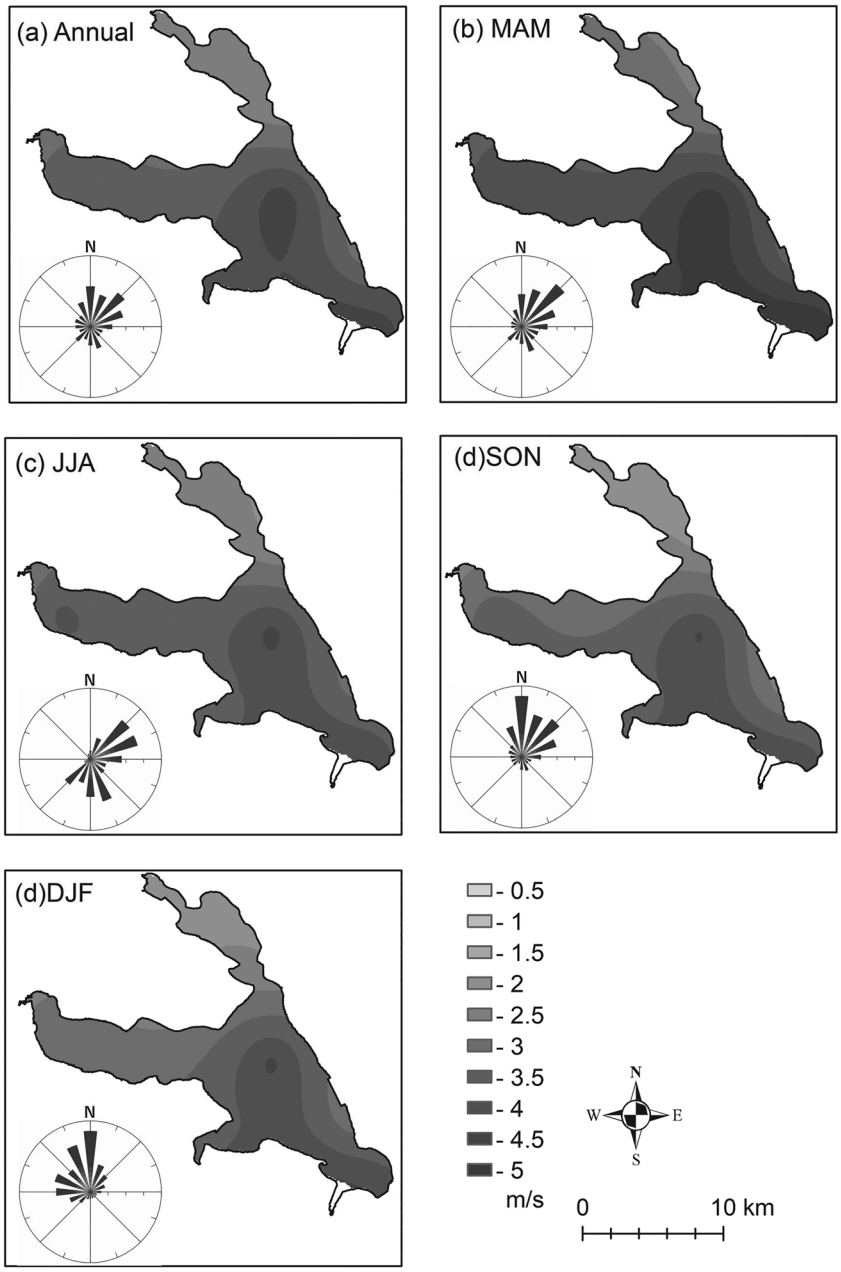

Figure 4. Spatial variation of 5-year averaged wind speed. (a) Annual means, (b) Spring (March-April-May), (c) Summer (June-July-August), (d) Fall (September-October-November), and (e) Winter (December-January-February). Dominant wind directions are also shown in each panel as a wind rose in which the frequency of the wind direction is given as relative value; the range of the radius axis is 0–20%.

regardless of wind conditions. This is also verified by smaller skewness and kurtosis under cloudy conditions. They tend to indicate that there are a fewer number of outliers and shorter tails in the probability distribution curve. Smaller CV values under cloudy condition can also be noticed for $T_s - T$ and $q_s - q$, but not for U. Thus, it appears that cloudiness suppresses spatial variability of $T_s - T$ and $q_s - q$. Wind speeds are not affected by cloudiness. Therefore, under clear conditions, both wind speed and vertical differences of temperature and humidity are important to control spatial variability of H and L_eE while wind speed becomes a dominant factor under cloudy conditions. Indeed, a comparison of maps of H and L_eE with those of $T_s - T$, $q_s - q$, and U (Figure 7 for the moderate wind speeds case) has indicated

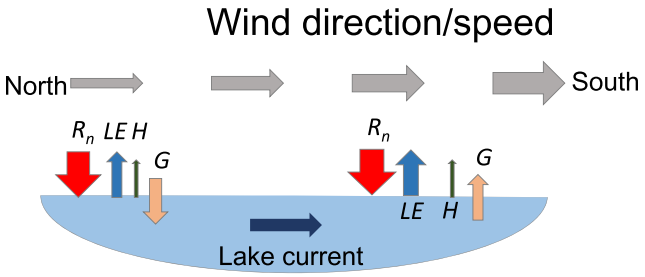

Figure 5. Schematic figure showing energy flow along the north-south cross-section over Lake Kasumigaura. Prevailing wind direction and relative wind speeds along the cross-section are also shown. Lake current is from INA (2008) observed under northerly wind direction.

that spatial variation of H and L_eE are similar to that of U but are not similar to that of $T_s - T$ or $q_s - q$. Over a long-term period such as a month or more, both clear and cloudy skies exist and therefore the nature of spatial variability is somewhere in between that of clear and cloudy conditions. In our study, we see characteristics of the cloudy condition more in the spatial variability of the seasonal, annual, and 5-year averaged fluxes.

3.2.3. Applicability of our Findings to Other Lakes

The results obtained in our study are primarily for Lake Kasumigaura, a shallow, 10^2-km^2 lake on a flat topography. A natural question arises whether the finding that the wind is a main driver of the EB spatial variability can be applied to other lakes in general. This is difficult to answer at the moment as there are not a sufficient number of similar lake studies to compare with our results. However, we can speculate to some extent what could cause the difference in spatial EB variability based on our general knowledge on the lake EB system.

Within Lake Kasumigaura, we found that wind speed U increased along the main wind direction. This was because it takes some distance for airflow to be adjusted to lake surface conditions after it passes the shoreline. This has been studied as a development of the IBL. Since this is a rough-smooth transition, U at given height should gradually increase along the wind direction until the airflow becomes fully adjusted. This adjusted layer is referred to as the internal equilibrium layer and occupies the depth h of the lowest 10% the IBL. The ratio of the height h to the distance x from the shoreline is typically 1/200 under neutral atmospheric stability condition (e.g., Brutsaert, 1982; Garratt, 1992). Thus, wind speed increase at 10 m height is expected from the shoreline till about 2 km offshore along the wind direction. This should be longer under stable condition, and shorter for the unstable condition. Figure 4 shows that the pronounced wind speed

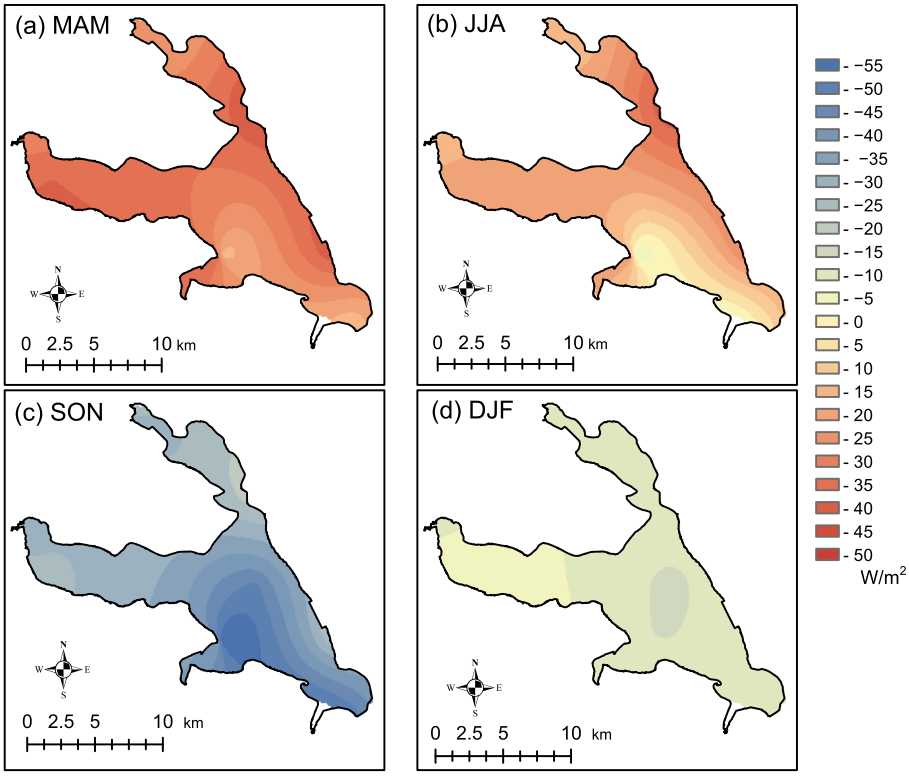

Figure 6. Spatial variation of 5-year averaged total seasonal energy flux into water body G over Lake Kasumigaura. (a) MAM represents spring (March-April-May); (b) JJA stands for June-July-August in summer; (c) SON is fall season (September-October-November), and (d) DJF is winter (December-January-February).

Table 4
Meteorological Conditions and Spatial Variability Over Lake Kasumigaura for Different Sky and Wind Conditions

Wind condition	Sky condition	Date and time (JST)	U (m/s)	Wind direction	T_s–T (°C)	q_s–q	H (W/m^2)	L_eE (W/m^2)
Moderate winds	Clear	21 Nov. 2007, 10:30	2.76 ± 0.63	NE to N	3.62 ± 0.71	0.00184 ± 0.00059	21.2 ± 5.4	24.7 ± 9.7
			0.23		0.20	0.32	0.25	0.39
			−0.80		−0.26	−0.15	2.06	0.64
			−0.26		2.67	1.15	14.79	3.19
	Cloudy	14 Dec. 2008, 9:00	2.73 ± 1.25	N	5.62 ± 0.92	0.00317 ± 0.00035	27.1 ± 3.2	38.1 ± 4.7
			0.46		0.16	0.11	0.12	0.12
			0.36		1.23	0.71	0.07	0.14
			−0.52		0.79	0.36	−0.88	−0.10
Weak winds	Clear	7 Dec. 2007, 10:30	0.85 ± 0.11	Variable	1.38 ± 0.73	0.00260 ± 0.00054	7.4 ± 4.7	20.4 ± 5.9
			0.13		0.53	0.21	0.64	0.29
			0.51		2.15	1.93	3.38	2.44
			0.91		12.9	8.38	21.04	13.54
	Cloudy	19 Nov. 2011, 9:00	1.10 ± 0.52	Variable	12.28 ± 1.57	0.00326 ± 0.00024	16.4 ± 2.7	26.5 ± 5.0
			0.48		0.13	0.07	0.16	0.19
			1.66		0.28	0.42	−1.07	−0.61
			2.43		0.50	1.68	1.37	0.66
Strong winds	Clear	1 Jan. 2009, 10:30	7.19 ± 1.68	NW to W	0.54 ± 0.71	0.00360 ± 0.00037	4.3 ± 5.4	81.9 ± 19.1
			0.23		1.29	0.10	1.25	0.23
			1.11		2.10	−0.40	2.41	0.61
			0.05		12.92	63.70	14.03	4.17
	Cloudy	20 March 2008, 12:00	8.39 ± 1.78	NE	4.69 ± 0.69	0.00332 ± 0.00041	46.5 ± 8.5	80.8 ± 11.4
			0.21		0.15	0.12	0.18	0.14
			−0.29		1.30	0.74	0.31	0.20
			−0.73		1.09	−0.56	−0.39	−0.44

Note. In each data column, the first row indicates the mean ± standard deviation; second row gives the coefficient of variation (CV), third row lists skewness, and fourth row the kurtosis.

change for $0 < x <$ 2–5 km. Thus, if the lake dimension is much larger than, say, 10 km, spatial variability is limited within small portions of the lake near the shoreline and the EB variability due to wind speed differences becomes less important.

On the other hand, if the lake size becomes larger, R_{sd} is expected to be less uniform and thus the difference of the incoming energy is expected to become a driver of spatial EB variability. Merinoa et al. (2001) determined the range in the semivariogram analysis of the hourly solar irradiance in western Nebraska in the United States. The range gives "zone of influence" (Sharma, 2009) and indicates the maximum distance where the spatial dependence occurs. In another word, beyond the distance given by the range, variables are not correlated. In western Nebraska, the range was around 200 km on the hourly irradiance field. Thus, if there is a lake with a horizontal scale larger than 200 km, the lake likely receives horizontally different incoming energy and has spatially variable EB. In fact, Lofgren and Zhu (2000) demonstrated that in Lake Huron the geographical difference of the progress of season (i.e., the spatial difference of incoming energy at any given moment) was the driving force of flux spatial variability. However, the range is probably different for different regions with various climates.

If the lake size becomes smaller, wind speed remains important for the EB spatial variability. R_{sd} is probably uniform, except for a lake in the mountain region where topography enhances spatial differences of

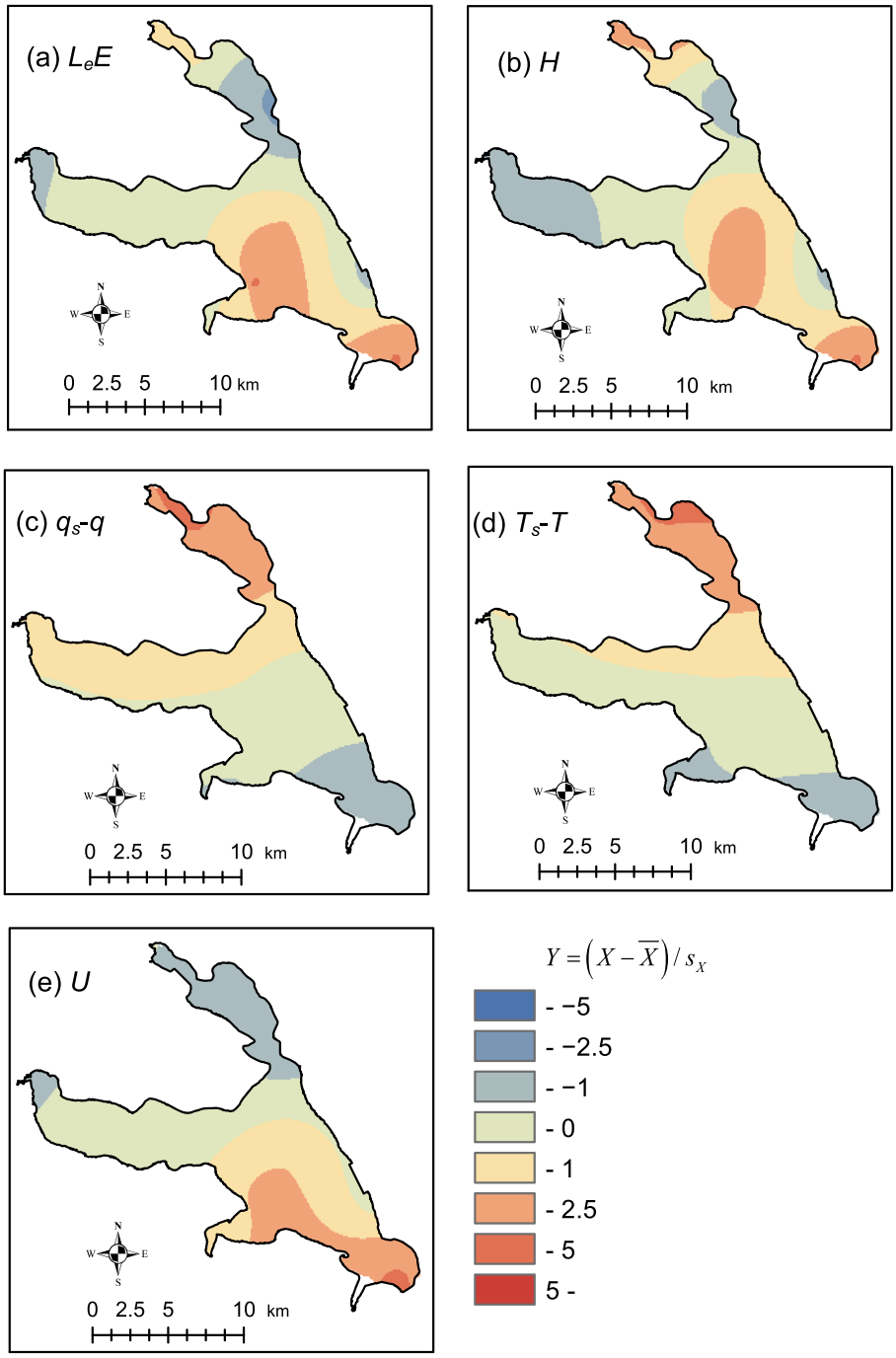

Figure 7. Spatial variation of (a) L_eE, (b) H, (c) $(q_s - q)$, (d) $(T_s - T)$, and (e) U at 9:00 JST, 14 December 2008 under cloudy condition. Variables x are shown as a nondimensional variable $y = (x - \overline{x})/s_x$ where $\overline{x}$ and s_x are the spatial average and the standard deviation.

incoming energy through shadowing and reflectance effects (e.g., Dubayah, 1994). In this case, even a small lake may exhibit a spatially variable EB due to the difference of the incoming energy.

Another important factor is the mixing process within a lake. In general, mixing should reduce spatial variability through advection and diffusion. In the case of Lake Kasumigaura, lake current was found to work that way through energy transportation along the dominant wind direction but was not strong enough to eliminate the spatial variability. Thus, whether or not there is spatial EB variation, and to what extent it exists

should depend on the balance between the driving force(s) of spatial variability and the mixing process. Mixing processes occur based on external energy and forces but are influenced by many factors such as shape, depth, size, the climatic region, as well as the presence of incoming rivers of a lake (e.g., Horne & Goldman, 1994), and therefore it is somewhat difficult to generalize the strength of the mixing process of a lake. Clearly more studies are needed to clarify this point particularly in relation to the driving force(s) of the spatial variability.

4. Conclusions

We have analyzed high-resolution (both in time and space) maps of surface EB over Lake Kasumigaura and found the surface fluxes to be spatially not uniform. Turbulent fluxes, particularly L_eE, are more variable than the radiative fluxes. The resulting G of the EB equation is also spatially variable. A main cause of such spatial variability is an uneven distribution of wind speed over the lake. Wind speeds increase over the fetch and, as a result, strong wind speed areas result in downwind regions. They are the regions with larger turbulent fluxes, and negative (upward) G values in contrast to the upwind regions with smaller turbulent fluxes and positive G. This spatial difference in G appears to be maintained through energy advection by lake currents along the wind direction. Our results, therefore, illustrate a need to treat lakes as two- or three-dimensional entity unlike present common practice of one-dimensional treatment in order to estimate the EB of a lake. In addition, we should pay more attention to the thermal regime within a lake as well as energy transportation by means of lake currents as a mechanism to maintain or dissipate nonuniform surface fluxes over a lake's surface.

Data Availability Statement

Meteorological data used in the analysis are available and were obtained from the Kasumigaura River Office, by the Lake Kasumigaura Water Research Station of the National Institute for Environmental Studies, by the Japan Meteorological Agency, by the National Institute for Environmental Studies, and by the Hyakuri Air Base of the Japan Air Self-Defense Force (Table S2). The data sets produced and used in this study (Sugita et al., 2020) are archived at the Hydroshare data repository (http://www.hydroshare.org/resource/9ee484df79e6471fb792c7910b25d57f).

Acknowledgments
We would like to thank the Kasumigaura River Office of the Kanto Regional Development Bureau, Ministry of Land, Infrastructure, Transport, and Tourism of Japan for allowing our measurements at the Koshin Observatory and for providing us with miscellaneous data sets. We appreciate constructive comments of three reviewers and associate editor which helped a lot to improve the quality of our manuscript. This work was supported and financed, in part, by the Japan Society for the Promotion of Science [grant KAKENHI 15K01159 and 20H01384]. Parts of this study were conducted while MS was at Kyoto University as a visiting professor.

References

Alcântara, E. H., Stech, J. L., Lorenzzetti, J. A., Bonnet, M. P., Casamitjana, X., Assireu, A. T., & Novo, E. M. L. M. (2010). Remote sensing of water surface temperature and heat flux over a tropical hydroelectric reservoir. *Remote Sensing of Environment*, *114*(11), 2651–2665. https://doi.org/10.1016/j.rse.2010.06.002

Blanken, P. D., Waynem, W. R., & Schertzer, W. M. (2003). Enhancement of evaporation from a large northern lake by the entrainment of warm, dry air. *Journal of Hydrometeorology*, *4*(4), 680–693. https://doi.org/10.1175/1525-7541(2003)004<0680:EOEFAL>2.0.CO;2

Brutsaert, W. (1982). *Evaporation into the Atmosphere*. Dordrecht: D. Reidel Pub.Co. https://doi.org/10.1007/978-94-017-1497-6

Cole, J. J., Prairie, Y. T., Caraco, N. F., McDowell, W. H., Tranvik, L. J., Striegl, R. G., et al. (2007). Plumbing the global carbon cycle: Integrating inland waters into the terrestrial carbon budget ecosystems. *Ecosystems*, *10*(1), 172–185. https://doi.org/10.1007/s10021-006-9013-8

DeBruin, H. A. R., & Keijiman, J. Q. (1979). The Priestley-Taylor evaporation model applied to a large, shallow Lake in the Netherlands. *Journal of Applied Meteorology*, *18*(7), 898–903. https://doi.org/10.1175/1520-0450(1979)018<0898:TPTEMA>2.0.CO;2

Downing, J., Prairie, Y., Cole, J., Duarte, C., Tranvik, L., Striegl, R., et al. (2006). The global abundance and size distribution of lakes, ponds, and impoundments. *Limnology and Oceanography*, *51*(5), 2388–2397. https://doi.org/10.4319/lo.2006.51.5.2388

Dubayah, R. (1994). Modeling a solar radiation topoclimatology for the Rio Grande River Basin. *Journal of Vegetation Science*, *5*(5), 627–640. https://doi.org/10.2307/3235879

Franz, D., Mammarella, I., Boike, J., Kirillin, G., Vesala, T., Bornemann, N., et al. (2018). Lake-atmosphere heat flux dynamics of a thermokarst lake in arctic Siberia. *Journal of Geophysical Research: Atmospheres*, *123*, 5222–5239. https://doi.org/10.1029/2017JD027751

Garratt, J. R. (1992). *The Atmospheric Boundary Layer Flow*. Cambridge: Cambridge University Press.

Hashimoto, H., Sagawa, T., Imai, T., & Fujita, K. (1985). Field study on movement of water in Kasumigaura. *Annual Journal of Hydraulic Engineering, JSCE*, *29*, 347–352. https://doi.org/10.2208/prohe1975.29.347 (in Japanese)

Hiyama, T., Sugita, M., & Kayane, I. (1995). Variability of surface fluxes within a complex area observed during TABLE 92. *Agricultural and Forest Meteorology*, *73*(3-4), 189–207. https://doi.org/10.1016/0168-1923(94)05074-G

Horne, A. J., & Goldman, C. R. (1994). *Limnology* (2nd ed.). New York: McGraw-Hill.

INA (2008). *Report on the Investigation of Lake Current of Lake Kasumigaura*. Tokyo: INA Corp. (in Japanese)

Li, Z., Lyu, S., Ao, Y., Wen, L., Zhao, L., & Wang, S. (2015). Long-term energy flux and radiation balance observations over Lake Ngoring, Tibetan Plateau. *Atmospheric Research*, *155*, 13–25. https://doi.org/10.1016/j.atmosres.2014.11.019

Lofgren, B. M. (1997). Simulated effects of idealized Laurentian Great Lakes on regional and large-scale climate. *Journal of Climate*, *10*(11), 2847–2858. https://doi.org/10.1175/1520-0442(1997)010<2847:SEOILG>2.0.CO;2

Lofgren, B. M., & Zhu, Y. (2000). Surface energy fluxes on the Great Lakes based on satellite-observed surface temperatures 1992 to 1995. *Journal of Great Lakes Research*, *26*(3), 305–314. https://doi.org/10.1016/S0380-1330(00)70694-0

Mammarella, I., Nordbo, A., Rannik, Ü., Haapanala, S., Levula, J., Laakso, H., et al. (2015). Carbon dioxide and energy fluxes over a small boreal lake in southern Finland. *Journal of Geophysical Research: Biogeosciences*, *120*, 1296–1314. https://doi.org/10.1002/2014JG002873

Merinoa, G. G., Jonesb, D., Stooksburyc, D. E., & Hubbardd, K. G. (2001). Determination of semivariogram models to krige hourly and daily solar irradiance in Western Nebraska. *Journal of Applied Meteorology*, *40*(6), 1085–1094. https://doi.org/10.1175/1520-0450(2001)040<1085:DOSMTK>2.0.CO;2

Muraoka, K. (1981). Water volume balance of Lake Kasumigaura, *Research Report from the National Institute for Environmental Studies*, No.20, 103-151. https://www.nies.go.jp/kanko/kenkyu/pdf/972020-1.pdf (in Japanese)

Muraoka, K., & Fukushima, T. (1981). Lake current of Kasumigaura (Nishiura), *Research Report from the National Institute for Environmental Studies*, No.19, 1-150. https://www.nies.go.jp/kanko/kenkyu/pdf/972019-1.pdf (in Japanese)

Naito, T. (2008). Interaction between and surface water and groundwater in Lake Kasumigaura, MS Thesis, Univ. Tsukuba (in Japanese).

Nordbo, A., Launiainen, S., Mammarella, I., Leppäranta, M., Huotari, J., Ojala, A., & Vesala, T. (2011). Long-term energy flux measurements and energy balance over a small boreal lake using eddy covariance technique. *Journal of Geophysical Research*, *116*, D02119. https://doi.org/10.1029/2010JD014542

Ogawa, S. (2018). Heat balance and heat distribution in Lake Kasumigaura, MS. Thesis, Univ. Tsukuba, (in Japanese).

Prats, J., Reynaud, N., Rebière, D., Peroux, T., Tormos, T., & Danis, P.-A. (2018). LakeSST: Lake Skin Surface Temperature in French inland water bodies for 1999–2016 from Landsat archives. *Earth System Science Data*, *10*(2), 727–743. https://doi.org/10.5194/essd-10-727-2018

Priestley, C. H. B., & Taylor, R. J. (1972). On the assessment of surface heat flux and evaporation using large-scale parameters. *Monthly Weather Review*, *100*(2), 81–92. https://doi.org/10.1175/1520-0493(1972)100<0081:OTAOSH>2.3.CO;2

Rimmer, A., Samuels, R., & Lechinsky, Y. (2009). A comprehensive study across methods and time scales to estimate surface fluxes from Lake Kinneret, Israel. *Journal of Hydrology*, *379*(1-2), 181–192. https://doi.org/10.1016/j.jhydrol.2009.10.007

Sharma, D. D. (2009). *Geostatistics with Applications in Earth Sciences* (second ed.). Heidelberg: Springer. https://doi.org/10.1007/978-1-4020-9380-7

Sugita, M. (2020). Spatial variability of the surface energy balance of Lake Kasumigaura and implications for flux measurements. *Hydrological Sciences Journal*, *65*(3), 401–414. https://doi.org/10.1080/02626667.2019.1701676

Sugita, M., Ikura, H., Miyano, A., Yamamoto, K., & Wei, Z. (2014). Evaporation from Lake Kasumigaura: Annual totals and variability in time and space. *Hydrological Research Letters*, *8*(3), 103–107. https://doi.org/10.3178/hrl.8.103

Sugita, M., Ogawa, S., & Kawade, M. (2020). Energy and radiation balance maps of Lake Kasumigaura, Japan (2008–2012), *HydroShare*, http://www.hydroshare.org/resource/9ee484df79e6471fb792c7910b25d57f

Thiery, W., Davin, E. L., Panitz, H.-J., Demuzere, M., Lhermitte, S., & van Lipzig, N. (2015). The impact of the African Great Lakes on the regional climate. *Journal of Climate*, *28*(10), 4061–4085. https://doi.org/10.1175/JCLI-D-14-00565.1

Verburg, P., & Antenucci, J. P. (2010). Persistent unstable atmospheric boundary layer enhances sensible and latent heat loss in a tropical great lake: Lake Tanganyika. *Journal of Geophysical Research*, *115*, D11109. https://doi.org/10.1029/2009JD012839

Wang, W., Xiao, W., Cao, C. C., Gao, Z., Hu, Z., Liu, S., et al. (2014). Temporal and spatial variations in radiation and energy balance across a large freshwater lake in China. *Journal of Hydrology*, *511*, 811–824. https://doi.org/10.1016/j.jhydrol.2014.02.012

Wei, Z., Miyano, A., & Sugita, M. (2016). Drag and bulk transfer coefficients over water surfaces in light winds. *Boundary-Layer Meteorology*, *160*(2), 319–346. https://doi.org/10.1007/s10546-016-0147-8

Woolway, R. I., Verburg, P., Lenters, J. D., Merchant, C. J., Hamilton, D. P., Brookes, J., et al. (2018). Geographic and temporal variations in turbulent heat loss from lakes: A global analysis across 45 lakes. *Limnology and Oceanography*, *63*(6), 2436–2449. https://doi.org/10.1002/lno.10950

Woolway, R. I., Verburg, P., Merchant, C. J., Lenters, J. D., Hamilton, D. P., Brookes, J., et al. (2017). Latitude and lake size are important predictors of over-lake atmospheric stability. *Geophysical Research Letters*, *44*, 8875–8883. https://doi.org/10.1002/2017GL073941

Yamamoto, K. (2014). Changes in watershed environments and water balance of Lake Kasumigaura from 1970s to present. MS Thesis, Univ. Tsukuba. (in Japanese)

Zhao, X., & Liu, Y. (2018). Variability of surface heat fluxes and its driving forces at different time scales over a large ephemeral lake in China. *Journal of Geophysical Research: Atmospheres*, *123*, 4939–4957. https://doi.org/10.1029/2017JD027437